Available online at www.sciencedirect.com
SCIENCE DIRECT
Polymer 46 (2005) 4480–4491
polymer
www.elsevier.com/locate/polymer

Morphology and mechanical and dynamic mechanical properties of linear and star poly(styrene-*b*-isobutylene-*b*-styrene) block copolymers

Tety Kwee, Stacy J. Taylor, Kenneth A. Mauritz*, Robson F. Storey

School of Polymers and High Performance Materials, The University of Southern Mississippi, Box 10076 Hattiesburg, MS 39406-0076, USA

Available online 21 March 2005

Abstract

The morphologies of solution cast linear and star poly(styrene-*b*-isobutylene-*b*-styrene) (SIBS) block copolymers, of ~0.3–0.33 polystyrene (PS) volume fraction, were investigated using transmission electron microscopy (TEM) and small angle X-ray scattering (SAXS) methods. The linear (L) and 4-arm star materials have hexagonal packed cylinder morphologies. TEM indicates more continuous domains for the 3-arm SIBS and SAXS indicates lamellar morphology. The diameters of the PS cylinders are 25–30 nm in all cases, but inter-domain distances increase in the order: L→3-arm star →4-arm star SIBS. Dynamic mechanical analysis shows a decrease of plateau modulus in the order L→3-arm →4-arm star. T_g for the PIB phase is independent of star-branching. T_g increases for the PS block phase from L- to 3-SIBS although T_g(PS) for 4-SIBS is not significantly greater than that of L-SIBS. A high temperature shoulder on the PIB block glass transition peak is associated with sub-Rouse motions. Tensile modulus is essentially the same for L- and 3-SIBS but considerably greater for 4-SIBS. Stress levels and energy-to rupture increase in the order: L-SIBS <3-SIBS <4-SIBS and this behavior is rationalized in terms of the covalent junction points, entanglements, and hard block domain reinforcement. The results of cyclic deformation studies of hysteresis vs. maximum percent strain per cycle are interpreted in terms of irreversible morphological rearrangements, chain slippage through entanglements, and the influence of degree of star branching on motional constraints. There is a permanent set that increases while the stress required to extend the sample to a given strain decreases with each cycle. For cycles of lower maximum strain, and before PS block domains are disrupted, microscopic deformation is viewed as somewhat reversible, accompanied by a measure of energy dissipated as a consequence of slow relaxation kinetics of chain rearrangement vs. rate of bulk deformation. At high strain, a major fraction of the energy loss is attributed to irreversible, longer ranged disruption of the PS domains leading to permanent morphological change and permanent set. Percent hysteresis for all three cases decreases—then increases—with increasing maximum percent strain per cycle. The initial decrease is thought of in terms of a progressive decrease in the entropy of stretched chains with consecutive extensions where the chains are increasingly less able to contribute to hysteresis until the PS domains become disrupted on a large scale, after which the curves begin to rise.

Keywords: Star block copolymer elastomers; Morphology; Mechanical properties

1. Introduction

Most commercial thermoplastic elastomers (TPE) are A-B-A type block copolymers (BCP). Owing to thermodynamic incompatibility between the two dissimilar A and B blocks, microphase-separated morphologies form that depend on the volume fraction of the hard phase containing A blocks, which often are polystyrene, and the B blocks, that have a very low T_g, form a continuous soft phase. The PS hard domains act as reversible crosslinks that allows for thermal processing. As the PS phase volume fraction increases, spherical→hexagonally packed cylinder (HPC)→lamellar morphologies can be realized in this order [1]. Annealing time/temperature, casting solvent type and the rate of solvent evaporation will influence morphology [2–5]. Most commercial A-B-A type BCPs, produced via anionic polymerization, generally contain polydiene as the elastomeric soft phase in the middle block, e.g. polybutadiene, polyisoprene [6]. A major problem within polydiene blocks is that the unsaturated double bonds are unstable against thermal oxidation and UV radiation. For these reasons, commercial polydiene containing BCPs are subjected to a hydrogenation process. Hydrogenation,

* Corresponding author.

0032-3861/$ - see front matter © 2005 Elsevier Ltd. All rights reserved.
doi:10.1016/j.polymer.2005.02.031

often conducted in a post-polymerization step, is relatively expensive, often resulting in incomplete saturation. Thus, alternative blocks, such as fully saturated polyisobutylene (PIB), which has efficient intermolecular packing, has been explored to improve these properties as well as impart barrier properties.

Recent advances in living carbocationic polymerization allow the production of well-defined PIB containing BCPs with controlled architectures that cannot be achieved through traditional anionic polymerization [7–9]. Multi-arm or star BCPs are considered the future generation of TPE materials since their mechanical properties and processing characteristics are often superior to those of linear BCPs as a result of improved hard domain dispersions [10]. Synthesis of multiarm BCPs involves routes ranging from 'linking' or 'arm-first'[11–15], to more sophisticated routes such as 'core-first' [10]. Commercial star polymers produced via the 'linking' method involve reacting the living anionic polymer chain ends with silane coupling agents [6]. Several disadvantages arise from this method; excess living anionic polymer chains are often necessary to force a complete linking reaction, and the number of target arms cannot be precisely controlled primarily due to steric effects [11,14]. Storey et al. have synthesized multi-arm star BCPs through subsequent addition of divinylbenzene (DVB) at the end of polymerization to allow the DVB terminated polymer chain ends to couple with the microgel core DVB in the 'arm-first' method [14,15]. However, this method is limited to wide molecular weight distribution of arms due to a lack of control in tailoring precise arm numbers. The final method involves the use of multi-functional initiators where the arms are grown directly from the center. This technique is particularly versatile in cationic polymerization since the majority of the chain ends exist in a dormant state allowing sufficient time for synthetic tailoring and precise control often required in star BCPs. One disadvantage of this method involves incomplete initiation resulting in a reduction of the desired target arms. Thus, characteristics of initiator species such as solubility, rate of initiation, and steric effects are important parameters in designing star BCPs [16]. Since the syntheses of the multifunctional initiators are often challenging and only a few types of multifunctional initiators essentially fulfill the above requirements, to this date, only a limited number of literature references involving the design of star BCPs based on the 'core-first' method has been documented.

Therefore, the primary focus of this paper is to evaluate the morphologies of linear, 3-, and 4-arm star poly(styrene-*b*-isobutylene-*b*-styrene) (SIBS) materials generated using multifunctional initiators, such as blocked dicumylchloride (bDCC), tricumyl chloride (TCC), and biphenyl tetracumyl chloride (BPTCC), and to relate these molecular architectures and morphologies to their mechanical properties. These are considered to be model studies involving solution cast materials. Future characterizations of structure and properties will be performed on melt-processed samples.

2. Experimental: block copolymer materials

The linear, 3-arm, and 4-arm star poly(styrene-*b*-isobutylene-*b*-styrene) (SIBS), labeled as L-SIBS, 3-SIBS, and 4-SIBS, were synthesized using initiators such as blocked dicumylchloride (bDCC), tricumyl chloride (TCC), and biphenyl tetracumyl chloride (BPTCC). The synthetic procedures and the initiators were described elsewhere and are omitted here [16]. Overall, the BCPs consist of PS in the outer block and PIB in the center block, and the target volume fraction of PS in each sample was kept within the range 0.30–0.33. The total MW of SIBS and MW of the PIB center block were analyzed using GPC, and the results are listed in Table 1. Shown in the GPC (RI) trace in Fig. 1, all samples possessed unimodal MW distributions. However, high MW shoulders were observed in the linear and 3-arm SIBS samples and this has been attributed to chain coupling reactions during end block propagation in the case where the active chain ends react with the *para*-position of the styrene repeat unit. UV analysis was also conducted to detect the presence of homo PS since the styrene repeat units contain chromophores that are sensitive to UV. A low molecular weight tail and peaks, not observed in the GPC (RI) traces, were detected in the linear and star SIBS, which suggested the presence of homo PS in the samples.

3. Experimental: block copolymer characterization

Approximately 4.0 g of SIBS was dissolved in 50 mL of THF. The polymer solutions were poured in Teflon pans and covered with aluminum foil to control the rate of solvent evaporation. The solutions were then cast at 60 °C in a casting oven for 2 days prior to annealing under vacuum at 110 °C for 4 days.

Table 1
Total and block molecular weights of linear and star poly(styrene-*b*-isobutylene-*b*-styrene) (SIBS) materials synthesized from multifunctional initiators

Sample	Initiator	M_w PIB center block (g/mol)[a]	M_w per arm (g/mol)	M_w total BCP (g/mol)	PS mass percent	PS volume percent
L-SIBS	bDCC	41,220	32,406	64,811	36.4	32.8
3-SIBS	TCC	78,500	40,568	121,705	35.5	31.9
4-SIBS	BPTCC	91,970	34,890	139,561	34.1	30.5

[a] M_w center block includes all of the arms.

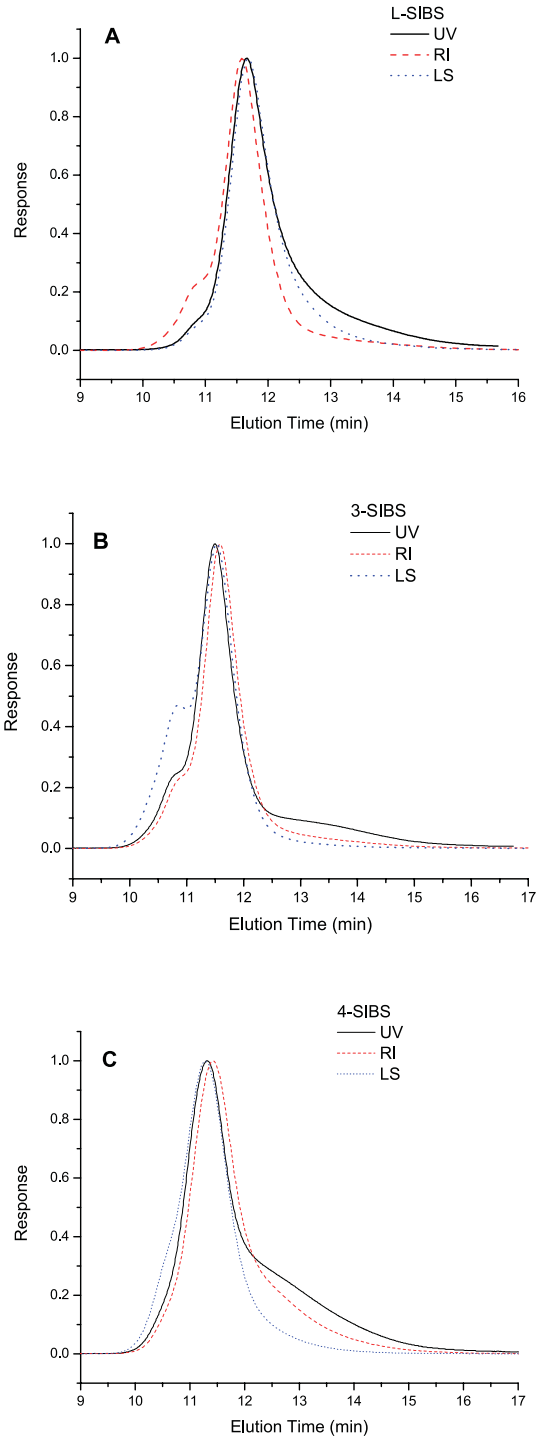

Fig. 1. SEC traces of (A) L-SIBS, (B) 3-SIBS, and (C) 4-SIBS.

Transmission electron microscopy (TEM) and small angle X-ray scattering (SAXS) analyses were used to examine the morphology of these materials. TEM micrographs were obtained be means of a Zeiss EM 109T microscope utilizing 50 keV accelerating voltage. All specimens were sectioned with both a glass knife and diamond knife using a Reicherd-Jung Ultracut E microtome at −80 °C. Each section was then transferred from the edge of the diamond knife to a 600 hexagonal mesh copper grid. The thickness of the sections was approximately 40–60 nm. Electron density contrast between the soft and hard block domains was imparted through staining the sections with ruthenium tetroxide (RuO_4). The dark and the bright regions shown in the TEM micrographs correspond to the PS and PIB domains, respectively.

SAXS measurements were conducted on the X3A2 beam line at the National Synchrotron Light Source at Brookhaven National Laboratories. The SAXS camera was configured with a 1.8 m sample-to-detector distance, and X-rays of wavelength 0.155 nm were used. Two-dimensional (2D) scattering data of the samples was collected using image plates. The collected scattering intensities were further corrected for absorption due to air scattering and thickness of the specimens based on a transmission factor calculated through beam monitoring using ionization chambers before and after the sample collection. The corrections for background scattering were performed using scattering from a blank sample holder. Q-scaling calibrations were conducted using a silver behenate standard. All analyses of the 2D scattering patterns were conducted using the Polar software developed by Stonybrook Technology and Applied Research, Inc. The SAXS profiles displayed consist of semi-logarithmic plots of absolute scattered intensity vs. magnitude of the scattering vector, q. The Bragg spacing (D_s) was derived from the position of the first-order lattice scattering peak at q^* using the equation $D_s = 2\pi/q^*$.

The dynamic viscoelastic storage modulus (E') and loss tangent = $\tan\delta = E'/E$ (E'' is the loss modulus) vs. temperature (T) curves for the linear and star SIBS samples were generated using a DMA Thermal Analysis Q800 system. Sample thickness was kept between 0.5 and 0.8 mm. All samples were run in tensile mode with a heating rate and frequency of 2 °C/min and 1 Hz, respectively.

Mechanical tensile stress vs. strain as well as mechanical hysteresis studies were conducted using a Material Testing System where dog bone shaped specimens were prepared according to ASTM specifications [17]. Strain is defined as $\varepsilon = (\Delta L)/L_0$, where ΔL is the change in the sample length upon extension or retraction, and L_0 is the sample gauge length. The strain rate in the tensile experiments reported here was 5 cm/min. Cyclic loading experiments were used to evaluate mechanical hysteresis and all samples were also subjected to a constant strain rate of 5 cm/min up to various, consecutively higher, strain levels followed by retraction until the stress returned to zero. Percent hysteresis ($H\%$) was calculated as the fraction of irreversible energy that was lost upon extension and retraction and was calculated based on the following equation:

$$H\% = \left[\frac{H_{\text{extension}} - H_{\text{retraction}}}{H_{\text{extension}}}\right] \times 100\%$$

As $H_{\text{extension}}$ and $H_{\text{retraction}}$ are the areas, in units of work, under the elongation and retraction curves, respectively,

$H_{extension} - H_{retraction}$ is the area bounded between these curves and is the mechanical energy lost per cycle.

It should be mentioned that all of the solution cast samples were prepared in the same way. For a given polymer type, samples from the same batch were used for all of the analyses. Therefore, meaningful correlations between structure and properties, regardless of analytical tool utilized, can be made.

4. Results and discussion

The morphology of L-SIBS is shown in the TEM micrograph in Fig. 2. There is clear hexagonal packed PS cylinder (HPC) morphology in which the cylinders are embedded in a continuous PIB matrix. The cylinder diameters are 25–30 nm and they are aligned rather perpendicular to the plane of the image.

The SAXS scattering profile of the same L-SIBS sample is seen in Fig. 3. The 2D scattering data show equal intensity along a ring pattern indicating isotropic orientation of the PS domains. The q peak positions of 1, 2, $\sqrt{7}$, ($\times q^*$) are characteristic of HPC morphology although the peak at $\sqrt{3}$ is missing, and these results are in harmony with the direct visualization provided by TEM as seen in Fig. 2. The inter-domain spacing D_s, is approximately 38.06 nm, which is commensurate with the spacings seen on the TEM micrograph. A slight shoulder at $q \sim 0.24\ nm^{-1}$ is located between the first and second peaks. The origin of this peak is unclear, but perhaps it is related to a trace amount of phase-segregated homopolystyrene; this suggestion is based on the low molecular weight tail in the UV trace seen in Fig. 1A.

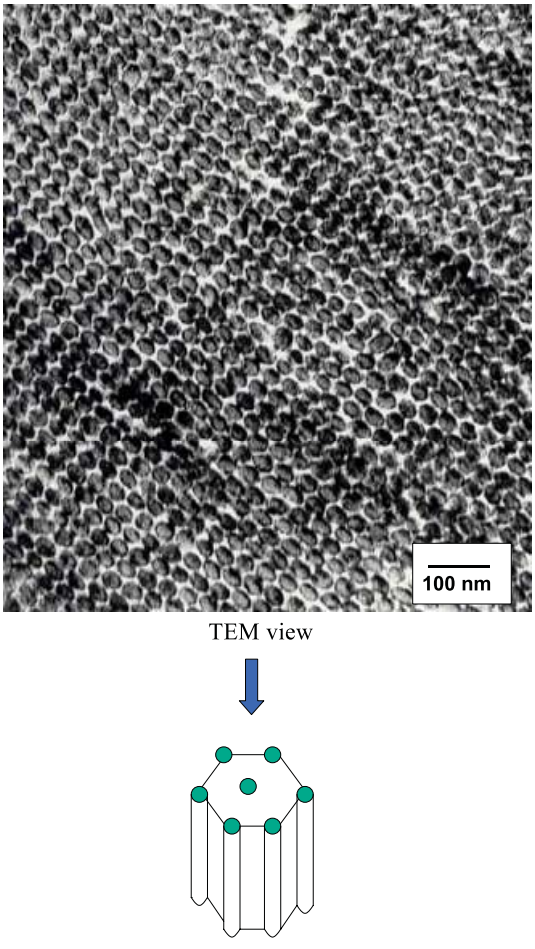

Fig. 2. TEM micrograph of an L-SIBS sample that illustrates HPC morphology.

The morphology of 3-SIBS is shown in the TEM micrographs in Fig. 4. The PS block domain sizes are again 25–30 nm. Spheres that may be of PS composition seen at high magnification (Fig. 4A) appear isolated and segregated throughout the entire sample. The larger scale morphology at lower magnification (Fig. 4B) shows PS block domains that are more continuous as compared to the morphology of linear SIBS, and in most cases, resembles lamellar morphology. In fact, the SAXS peak sequence for this same sample, at 1, 2, 3, and 4 ($\times q^*$) (Fig. 5) also reinforces the suggestion of lamellar morphology with long-range order.

Referring again to evidence in the GPC UV trace (Fig. 1B), incorporation of a significant degree of low molecular weight homopolystyrene could affect an increase in the overall PS composition volume fraction that causes a morphological shift from HPC to lamellae as depicted in Fig. 6. Fig. 6A shows the usual equilibrium HPC morphology for this PS block volume fraction in the copolymer. The added homopolystyrene is viewed as preferentially segregating into the existing PS block domains (Fig. 6B) which become distorted so that some of the cylinders become interconnected with the majority retaining their cylindrical shapes (Fig. 6C). With further addition of homopolystyrene, these domains become increasingly interconnected with only a few distinct cylinders remaining (Fig. 6D), and a lamellar morphology ultimately forms (Fig. 6E). Consequently, the SAXS data will no longer reflect a cylindrical array. It is seen that $D_s \sim 43.75$ nm, which is larger than that for L-SIBS. A rationalization of increasing D_s should account for the fact that the PS blocks in the 3-arm star are more restricted.

The TEM micrograph in Fig. 7, and SAXS profile in Fig. 8, of the 4-arm star SIBS indicate HPC morphology. Using TEM, the cylinders formed by 4-SIBS molecules show less structural order than L-SIBS and the size of the PS block domains is, again, 25–30 nm. However, the SAXS peaks that appear at the relative positions of 1, 2, $\sqrt{7}$, reflect an HPC microstructure, although the peak at $\sqrt{3}$ is missing. D_s for 4-SIBS was calculated to be ~ 59.17 nm, which is larger than the values for both L-SIBS and 3-SIBS. Table 2 shows the progressive increase of D_s in the order: linear → 3-arm star → 4-arm star SIBS. Perhaps, this progression is caused by a decreasing degree of chain mobility as more chains are tethered to a hub and this, in turn, would impede the kinetics and limit chain conformations during the drive toward equilibrium morphology. In the worst case, the motions of a

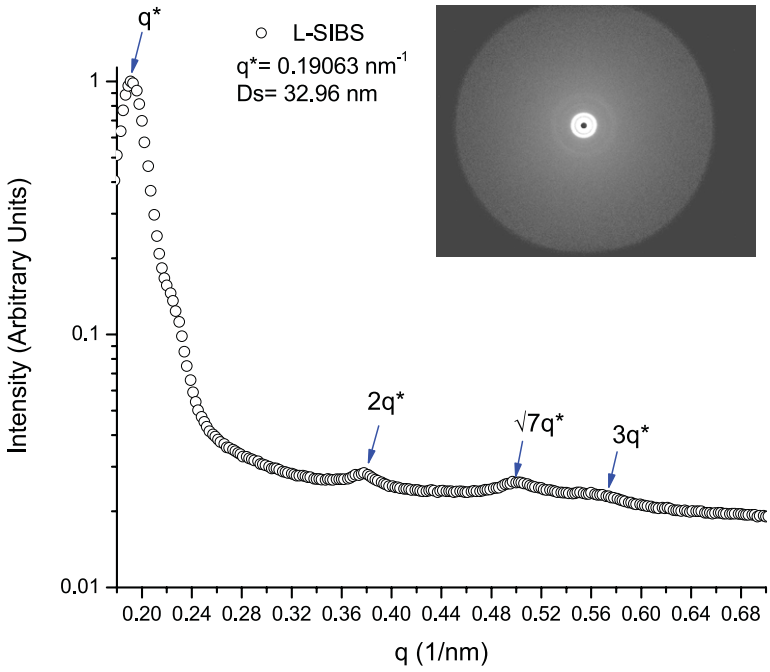

Fig. 3. SAXS profile for L-SIBS. $q^* = 0.1906\ \mathrm{nm}^{-1}$.

given arm in a four arm star molecule are coupled to the motions of the three other arms and this can be thought of as an enhanced energy barrier for chain-arm self-assembly.

Plots of E' and tan δ vs. T for the three SIBS molecular architectures are shown in Fig. 9. On the E' plots, a rubbery plateau exists for each case over approximately the same temperature range between two glass transitions. The plateau modulus, interestingly, decreases in passing from linear → 3-arm → 4-arm architectures. Perhaps, this is related to an increasing number of PIB segments in the center block in passing from the linear to star blocks. More statistical conformations can be sampled as the PIB blocks

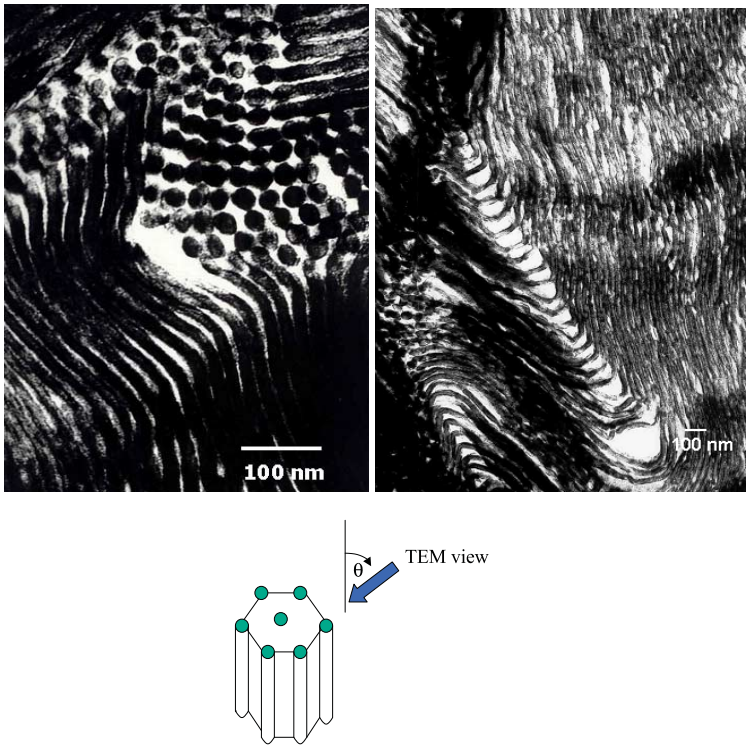

Fig. 4. TEM micrographs of a 3-SIBS sample at (A) high and (B) low magnification.

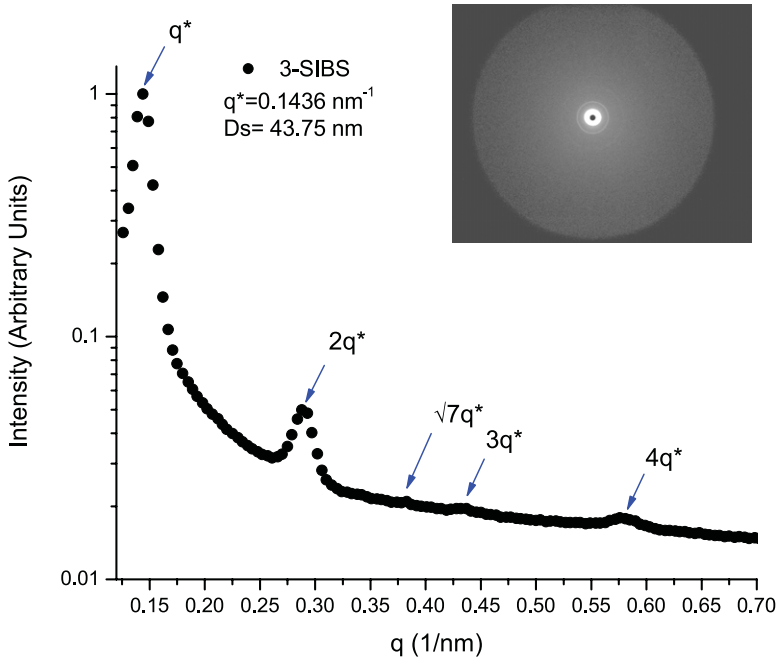

Fig. 5. SAXS profile of the same 3-SIBS sample as in Fig. 4. $q^* = 0.1436\ \mathrm{nm}^{-1}$.

become longer and this entropy factor affects the resistance to deformation in this phase. As seen in Table 1, while the PS phase volume fraction in each of all three block copolymers is essentially the same, the materials differ in terms of molecular weight, which becomes greater with degree of star branching. The molecular weight of the PIB segments in 4-SIBS is more than twice that in the linear block.

The peak temperatures of the two glass transitions that appear on the tan δ plots are listed in Table 3. T_g for the PIB phase, at $\sim -52\,^{\circ}$ C, appears to be independent of star-branching. Thus, long-range segmental motion in the soft blocks does not seem to be impeded by their being linked together at a hub. The dielectric relaxation studies of multi-arm *cis*-polyisoprene star molecules, of Boese, Kremer and Fetters, seem to be in harmony with these results [18,19]. Their studies found that molecular motion in one arm was practically independent of those in the other arms. However, this fact does not explain the downward shift in the rubbery plateau modulus with increased star branching and a more

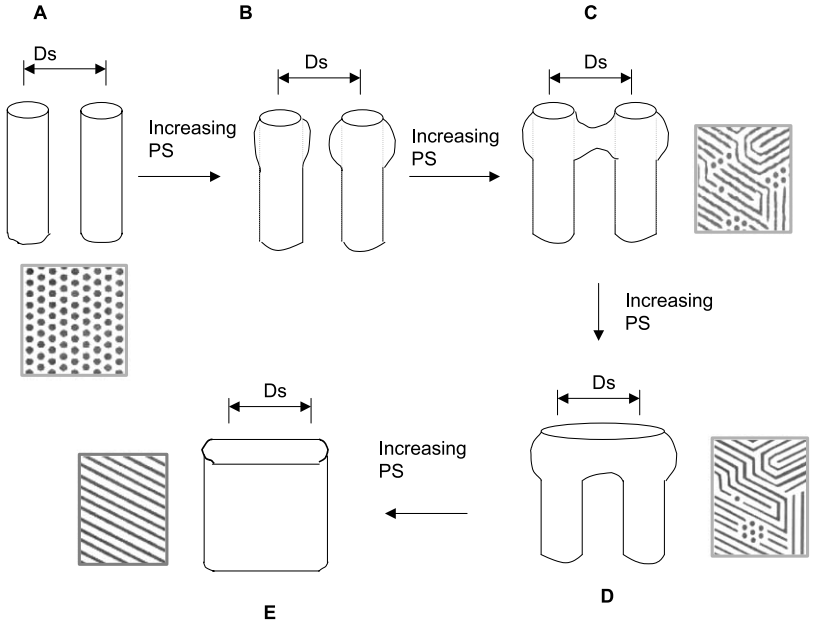

Fig. 6. Proposed scheme of morphology shift from HPC to lamellae upon addition of homopolystyrene molecules to the PS block domains of 3-SIBS.

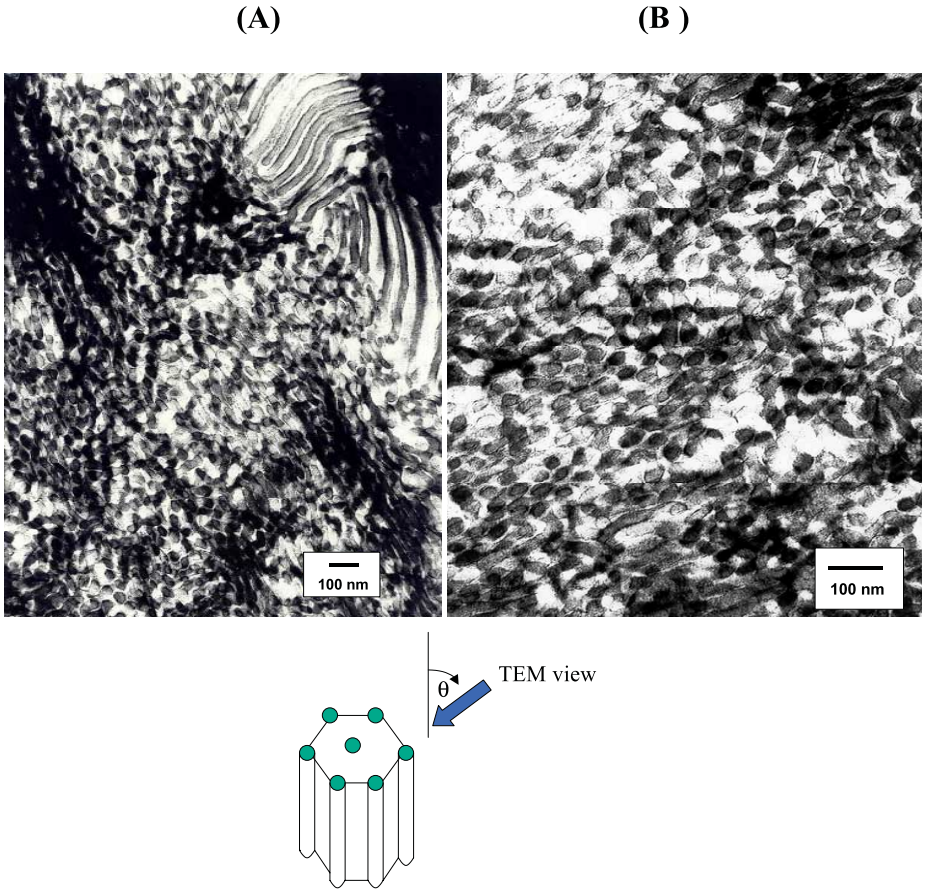

Fig. 7. TEM micrographs for a 4-SIBS sample at (A) low and (B) high magnification.

detailed look at the region about the PIB glass transition would seem to be necessary.

In the scheme depicted in Fig. 10, only cohesive PS domains act as crosslinks in L-SIBS, whereas, additionally, covalent PIB block junctions serve as permanent crosslinks in 3-SIBS as long as the PS domains remain intact. For the

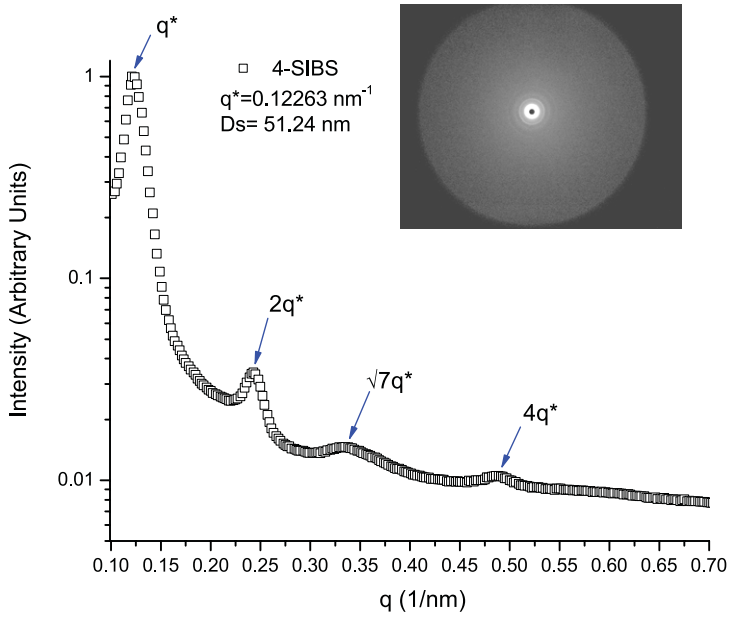

Fig. 8. SAXS profile of 4-SIBS with $q^* = 0.12263\ \mathrm{nm}^{-1}$.

Table 2
Morphology and inter-domain distances (D_s) in linear and star SIBS block copolymers based on TEM and SAXS analysis

Block Architecture	Morphology (TEM)	Morphology (SAXS)	Domain Size (nm)	q^* (nm^{-1})	D_s (nm)
L-SIBS	HPC	HPC	25–30	0.19063	38.06
3-SIBS	HPC/more interconnected PS domains	Lamellae	25–30	0.14360	43.75
4-SIBS	HPC	HPC	25–30	0.12263	59.17

same PS volume fraction, the PS blocks are more dispersed for the 3-SIBS material, thereby accounting for the lower E' values for the star branched materials.

The tan δ vs. T curves display a high temperature transition that corresponds to the glass transition for the PS phase and the peak temperatures for this relaxation are listed in Table 3. There is a considerable increase of T_g(PS) from L-SIBS to 3-SIBS (~106 °C to ~112 °C). Perhaps, this is due to the fact of having more continuous PS domains as seen in the TEM micrograph, that result from the incorporation of homopolystyrene. However, T_g(PS) for the 4-SIBS sample (~108 °C), is not significantly greater than that of L-SIBS. These results correlate with the fact that both L-SIBS and 4-SIBS have the same type of morphology, but the morphology of 3-SIBS is different.

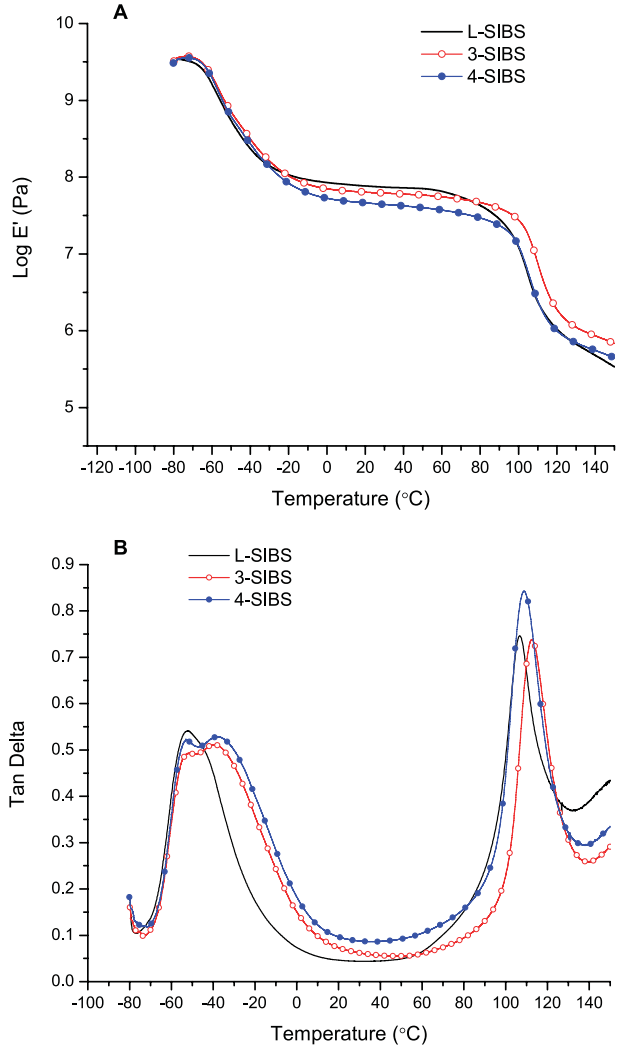

Fig. 9. (A) E' vs. T and (B) tan δ vs. T for L-SIBS, 3-SIBS and 4-SIBS samples.

There is a third transition, that is stronger for 3-SIBS and 4-SIBS than for L-SIBS, that appears at approximately −30 °C as a high temperature shoulder on the relaxation associated with the PIB block T_g. It is reasonable to associate this feature with the sub-Rouse mode relaxation associated with PIB homopolymers [20]. This relaxation is intermediate in both length and time scales between the fast segmental and the Rouse modes. The Rouse segment is defined as a section of a polymer chain that is long enough such that the distribution of end-to-end distance approximates a Gaussian probability distribution [21]. On the other hand, segmental relaxation associated with the glass transition primarily involves the correlated motions of only a few bonds in the backbone [22]. While Rouse segmental motions occur at longer time scales compared to local segmental motion, the sub-Rouse relaxation involves segmental motion with larger length scales but involving less repeat units than the shortest of the Gaussian submolecules as defined by the Rouse model [20,22]. Based on photon correlation spectroscopy, Plazek and co-workers saw two separate transitions and attributed the relaxation process at a shorter time scale to local segmental motion, while the shoulder was attributed to a relaxation at a longer time scale, i.e. sub-Rouse mode [20]. Thus, the sub-Rouse mode is activated at a higher temperature as is seen on the tan δ vs. T curves.

The resolution and relative intensity of the T_g-related and sub-Rouse peaks are different for the linear and star blocks. As shown in the tan δ curves, the sub-Rouse relaxation occurs at higher temperatures for 3- and 4-SIBS than that for L-SIBS. The two peaks for L-SIBS, for which the PIB block molecular weight is the lowest, are harder to resolve, indicating that the two relaxations merge, as is known to occur for PIB homopolymers. While the long range segmental motions operative at T_g are independent of

Table 3
Glass transition temperatures for the PS and PIB block domains in linear and star block copolymers

Block architecture	T_g PIB (°C)	T_g PS (°C)
L-SIBS	−52.3	106.6
3-SIBS	−52.6	112.7
4-SIBS	−52.5	108.8

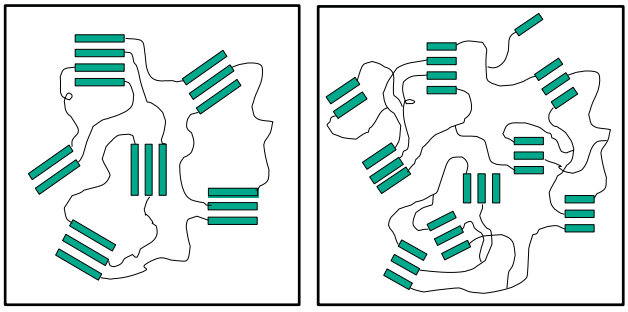

Fig. 10. Depictions of linear and 3-arm star BCP morphologies. While PS volume percent is the same for both cases, the total molecular weight of 3-SIBS is 1.88 times that for L-SIBS.

chain branching, the sub-Rouse process does depend on, and are decoupled from the Rouse modes, with branching.

Tensile stress vs. strain curves for the L-, 3- and 4-SIBS samples are seen in Fig. 11. The initial modulus is essentially the same for L-SIBS and 3-SIBS but is considerably greater for 4-SIBS, as seen in Table 4. These facts do not correlate with the glass transition in either block. The stress levels over the entire range of strains increase in the ordered progression: L-SIBS < 3-SIBS < 4-SIBS. The large values for elongation-at-rupture and the general curve features are characteristic of crosslinked rubbery materials. Energy-to-rupture, i.e. the total area under the curves, increases with increased star branching. Similar behavior was observed in earlier studies for other linear and 3-arm SIBS materials where both samples displayed nearly equal elongation-at-rupture, and this was attributed to strain-induced crystallization at high strains [23]. While strain-induced crystallization might be operative at the highest strains, the overall behavior seen in Fig. 11 is rationalized in terms of the permanent crosslinks in the form of the junction points for the PIB blocks, entanglements in the usual sense, and hard block domain reinforcement. It is considered that the PIB block junctions in the star molecules distribute the applied stress more uniformly to the hard PS domains in contrast with the linear molecules. The increasing concentration of PS domains will lead to more uniformly dispersed physical crosslinks that will affect more effective stress transfer throughout the bulk. These ideas were related in an earlier study by Shim and Kennedy who investigated the properties of similar star block copolymers consisting of PS-PIB arms emanating from cyclosiloxane cores [24]. These investigators found that the tensile properties of the star materials were better than that for the linear material for comparable arm compositions and molecular weights and tensile strength increased with increasing number of arms.

Cyclic tensile deformation was used to evaluate mechanical hysteresis as a function of maximum strain per consecutive cycle. Hysteresis is viewed as caused by irreversible morphological rearrangements and chain slippage through entanglements and the extent of this process would depend on the time scale of the experiment in the usual sense. A typical family of curves generated from experiments for L-SIBS is shown in Fig. 12. Upon retraction to zero stress for each cycle, there is a permanent set that increases with each cycle. There is a distinct shoulder on the extension curves, which suggests that the PS domains undergo uniaxial orientation and that these domains are deformed at the end of each cycle. The intensity of such a shoulder was seen to be proportional to the overall PS volume fraction by Diamant and co-workers in studies of a similar poly(styrene-*b*-butadiene-*b*-styrene) system, where the intensity of these shoulder peaks disappear as the PS volume fraction is reduced from 0.48 to 0.27 [25]. During each consecutive cycle, the stress required to extend the sample to a given strain decreases, and this behavior is known as 'stress softening' [26]. The PS hard domains,

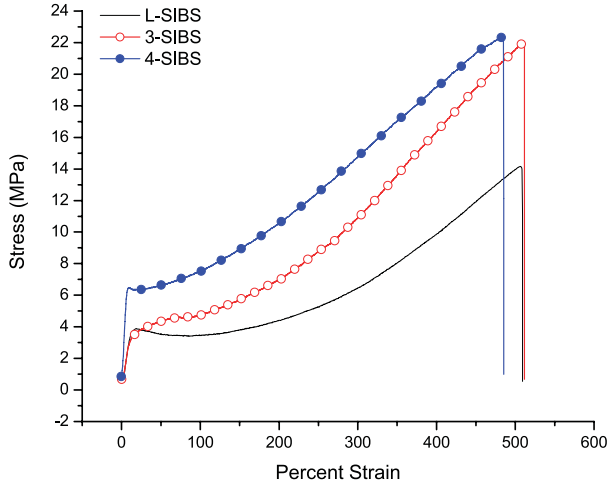

Fig. 11. Mechanical tensile stress vs. strain for linear and star SIBS samples at an extension rate of 5 cm/min.

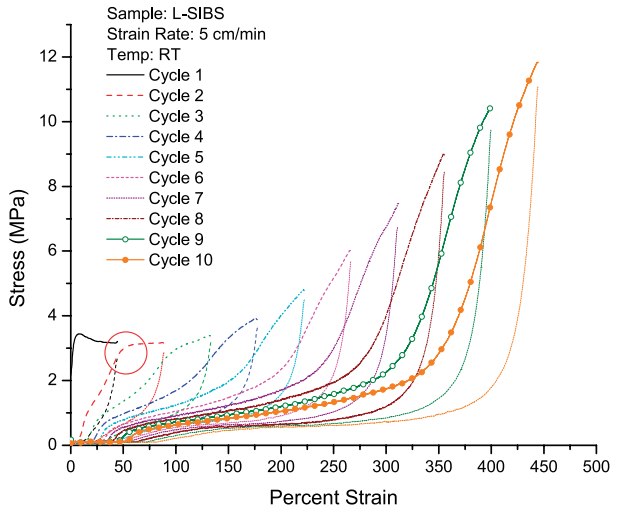

Fig. 12. Consecutive loading cycles for increasing maximum percent strain, at room temperature, for L-SIBS with a 5 cm/min strain rate. A 'shoulder' on the extension curve for the second cycle is identified by the circle.

Table 4
Tensile modulus, strain and stress-at-break for the three block copolymer molecular architectures

BCP architecture	Modulus (MPa)	Strain-at-rupture (%)	Stress-at-rupture (%)	Energy-to-rupture ($\times 10^3$ J/m^3)
L-SIBS	31.8	506.9	14.2	33.80
3-SIBS	32.2	511.0	22.0	53.75
4-SIBS	99.7	483.5	22.4	62.86

acting as physical crosslinks, are progressively disrupted as the result of successive extension at increasing strain levels, to a degree where the PS chains become increasingly 'mixed' in the soft PIB matrix. Weakening of these physical crosslinks, especially at high degrees of loading, is accompanied by energy dissipation in the form of intermolecular 'friction' in the sense that intermolecular interactions are disrupted as the chains slip past each other. Upon large deformation, the chains are stretched to the extent that they cannot return to their equilibrium configurations and different blocks have difficulty in separating into distinct phases. This is viewed as the cause of the permanent set seen in the retraction curves [27].

A microstructural view of deformation is illustrated in Fig. 13. Initially, the orientation of the PS block domains is random, i.e. isotropic. At lower extension, the flexible PIB blocks are stretched along the applied deformation direction such that the PS inter-domain spacings increase. At this point, the PIB chains, which are tethered to cohesive PS block domains, are largely able to recover their original statistical configurations after the external stress is removed, with some irreversibility. The rate at which this recovery occurs should be related to the kinetics of chain reptation. However, for larger deformations, the PIB chains are so extended that they exert considerable force on the PS blocks so that their domains become increasingly oriented. Ultimately, these forces increase to where the PS blocks are pulled from their domains and across interfaces leading to non-recoverable plastic deformation where the PS chains become increasingly mixed or diluted in the PIB matrix. Pakula and co-workers suggested that in order to displace PS chains across the interphases and mix with the PIB matrix, the system has to overcome a potential energy barrier related to the heat of mixing of the hard and soft blocks [27].

Since the hard domains are more dispersed, and may have a higher surface:volume ratio in the star materials, PS hard domain deformation that leads to non-recoverable overall plastic deformation is expected to occur at lower strain levels than in the case of L-BCP. This is seen in the plot of the normalized $H_{\%}$ vs. maximum percent strain curves in Fig. 14. A curve at a given temperature is 'normalized' in terms of the $H_{\%}$ value for the first cycle in that values for subsequent cycles are divided by the value for the first cycle. Thus, all of the modified curves begin at an $H_{\%}$ value of 1.00.

In the range of lower maximum percent strain, and before the PS block domains are disrupted, the deformations are viewed as somewhat reversible accompanied by a measure of energy dissipated as a consequence of the relaxation kinetics of chain rearrangement being slow relative to the rate of bulk sample deformation. At high strain, a major fraction of the energy loss is attributed to irreversible and longer ranged disruption of the PS domains leading to permanent morphological change and the observed permanent set [28]. As shown in Fig. 14, the lowest relative $H_{\%}$ values lie along the L-SIBS curve over the entire range of percent maximum strain. The values are greater for the star

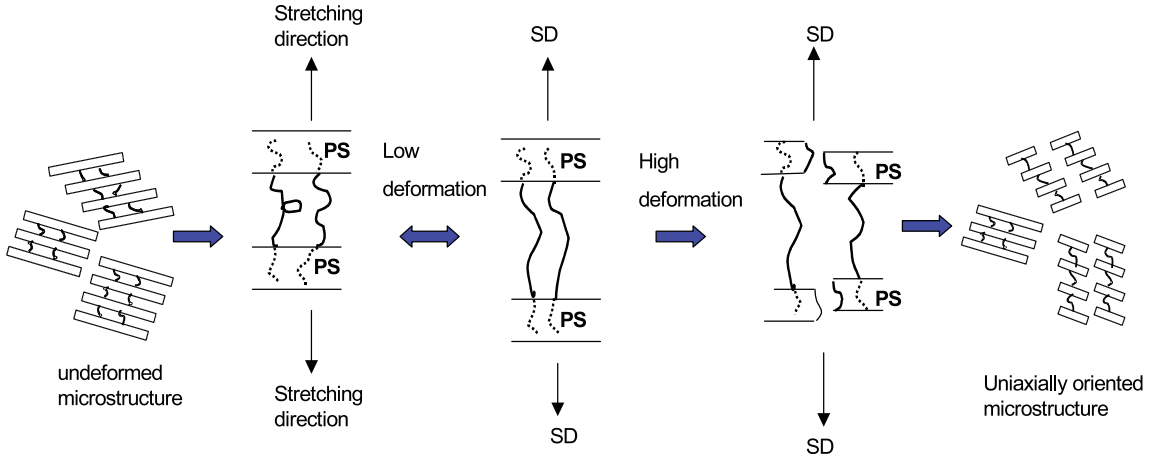

Fig. 13. Proposed scheme for progressive L-SIBS block rearrangement as the result of cyclic tensile deformation.

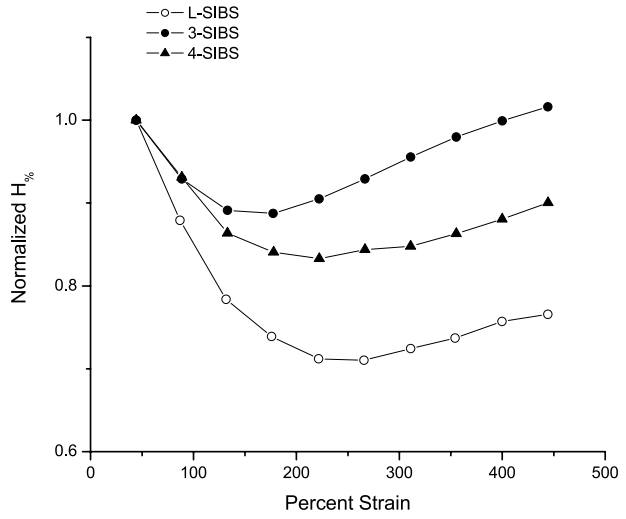

Fig. 14. Normalized percent hysteresis vs. maximum percent strain per cycle for linear and star SIBS materials.

architectures, the greatest being for 3-SIBS. The curve for L-SIBS shows the greatest sensitivity to percent strain and perhaps this is due to fewer constraints on chain motions and structural recovery as those posed by the PIB block junctions in the star molecules. This behavior is also consistent with the view of PS hard domains, in the star materials, that are more dispersed. These domains would be less stable in the star materials although the material is more interconnected so that there can be more mechanical energy dissipated over longer ranges upon deformation.

Each curve in Fig. 14 is characterized by a minimum that is positioned at a greater maximum percent strain for the linear than for the star materials. The initial decrease in $H_{\%}$ is viewed in terms of increased reversibility involving chain stretching-retracting when the overall morphology is reversible. As the number of arms increases, the evidence is that one domain dimension remains the same while the inter-domain spacing increases. This, in harmony with the GPC information on PIB block lengths, means that the PIB phase is of greater relative extent in the star as compared to the L-SIBS material. Consequently, for the star molecules, in which the PIB chain sections are coupled, there would be more entanglements involved in macromolecular rearrangements during extension and retraction so that more fractional energy would be dissipated. The overall initial decrease in $H_{\%}$ might be thought of as a progressive decrease in the entropy of stretched chains with every consecutive extension. As the entropy decreases the chains are increasingly less able to contribute to hysteresis until the PS domains become disrupted on a large scale, at which point the $H_{\%}$ curves begin to rise.

The $H_{\%}$ values of 3-SIBS are larger compared to the 4-SIBS perhaps owing to the more continuous PS domains as seen in the TEM micrographs. This could have the consequence of energy being dissipated over longer ranges that is manifest in higher energy dissipation.

5. Conclusions

The goal of this work was to investigate the morphology and mechanical, and viscoelastic properties of linear and star SIBS materials in which the PS volume fraction was ~0.3–0.33.

Based on TEM and SAXS analyses, linear and 4-arm star SIBS materials show hexagonal packed cylinder morphologies. For 3-SIBS, TEM shows more continuous domains and SAXS indicates lamellar morphology, likely due to residual homopolystyrene. The diameters of the PS cylinders are 25–30 nm in all cases, but inter-domain distances increase in the order: L → 3-arm star → 4-arm star. Perhaps, this progression is caused by a decreasing degree of chain mobility as more chains are tethered to a hub so as to impede the kinetics, and limit chain conformations, during the drive toward equilibrium morphology.

DMA shows a progressive decrease of plateau modulus in passing from L → 3-arm → 4-arm star architectures. Perhaps, this is caused by increasing PIB block molecular weight or/and PS domains that are more dispersed in the star materials.

T_g for the PIB phase is independent of star-branching, which shows that segmental motion in the soft blocks is not impeded by being linked together at a hub. There is considerable T_g increase for the PS block phase from L-SIBS to 3-SIBS perhaps due to homopolystyrene incorporation, although T_g(PS) for the 4-SIBS sample is not significantly greater than that of L-SIBS. A third transition in the form of a high temperature shoulder on the PIB block glass transition peak is associated with the sub-Rouse mode relaxation.

Initial tensile modulus is essentially the same for L- and 3-SIBS, but considerably greater for 4-SIBS. Stress levels over the entire range of strains and energy-to-rupture increase in the order: L- < 3- < 4-SIBS. While strain-induced crystallization might operate at the highest strains, overall behavior is rationalized in terms of the covalent junction points for the PIB blocks, entanglements, and hard block domain reinforcement. It is considered that PIB block junctions in the star molecules distribute stress more uniformly to the hard PS domains in contrast with the linear molecules.

Cyclic tensile deformation was used to study hysteresis vs. maximum percent strain per cycle and the results are interpreted in terms of irreversible morphological rearrangements, chain slippage through entanglements, and the influence of degree of star branching on motional constraints. There is a permanent set that increases while the stress required to extend the sample to a given strain decreases with each cycle.

In the range of lower maximum percent strain, and before PS block domains are disrupted, microscopic deformation is viewed as somewhat reversible accompanied by a measure of energy dissipated due to the relaxation kinetics of chain rearrangement being slow relative to the rate of bulk

deformation. At high strain, a major fraction of energy loss is attributed to irreversible and longer ranged disruption of PS domains leading to permanent morphological change and permanent set. Percent hysteresis for all three cases decreases—then increases—with increasing maximum percent strain per cycle. The initial decrease is thought of in terms of a progressive decrease in the entropy of stretched chains with consecutive extensions where the chains are increasingly less able to contribute to hysteresis. Eventually, the PS domains become disrupted on a large scale, after which the curves begin to rise.

While these polymers are considered to be model systems, future studies will involve melt-processed samples and the results will be compared to those for the solution cast samples reported here.

Acknowledgements

This work was supported by the US Army Research Office (DAAD19-01-0498 and DAAD04-96-1-0191) as well as the Mississippi DOD/EPSCoR program. Alan Phillips and Kirt Page, at the University of Southern Mississippi, conducted the SAXS experiments.

References

[1] Hashimoto T, Shibayama M, Fujimura M, Kawai H. Block copolymers. New York: Harwood Academic; 1983. p. 74.
[2] Kim G, Libera M. Macromolecules 1998;31:2569.
[3] Funaki Y, Kumano K, Jinnai H, Yoshida H, Kimishima K, Tsutsumi K, et al. Polymer 1999;40:7147.
[4] Sakurai S, Momii T, Taie K, Shibayama M, Nomura S, Hashimoto T. Macromolecules 1993;26:485.
[5] Quintana JR, Janez MD, Hernaez E, Garcia A, Katime I. Macromolecules 1998;31:6865.
[6] Southwick JG, Vonk W. Chem Eng 2002;50.
[7] Storey RF, Chisholm BJ, Masse MA. Polymer 1996;37(14):2925.
[8] Storey RF, Chisholm BJ. Macromolecules 1993;26:6727.
[9] Li D, Faust R. Macromolecules 1995;28:4893.
[10] Shim JS, Kennedy JP. J Polym Sci Part A: Polym Chem 1999;37:815.
[11] Frater DJ, Mays JW, Jackson C, Sioula S, Efstradiadis V, Hadjichristidis N. J Polym Sci Part B: Polym Phys 1997;35(4):587.
[12] Lee C, Gido SP, Pitsikalis M, Mays JW, Tan NB, Trevino SF, et al. Macromolecules 1997;30:3732.
[13] Bi L, Fetters LJ. Macromolecules 1976;9:732.
[14] Storey RF, Shoemake KA, Chisholm BJ. J Polym Sci Part A: Polym Chem 2003;34:1996.
[15] Storey RF, Shoemake KA. J Polym Sci Part A: Polym Chem 1999;37:1629.
[16] Taylor SJ. PhD dissertation; 2003, University of Southern Mississippi.
[17] ASTM D. 1708; 1993, 374.
[18] Boese D, Kremer F, Fetters LJ. Makromol Chem Rapid Commun 1988;9:367.
[19] Boese D, Kremer F, Fetters LJ. Macromolecules 1990;23:1826.
[20] Rizos AK, Ngai KL, Plazek DJ. Polymer 1997;38(25):6103.
[21] Inoue T, Osaki K. Macromolecules 1996;29:1595.
[22] Santangelo PG, Ngai KL, Roland CM. Macromolecules 1993;26:2682.
[23] Storey RF, Chisholm BJ, Lee Y. Polymer 1993;34:4330.
[24] Shim JS, Kennedy JP. J Polym Sci: A: Polym Chem 1999;37:815.
[25] Diamant J, Williams MC. Polym Eng Sci 1989;29(4):235.
[26] Beck RA, Truss RW. J Appl Polym Sci 1999;71:959.
[27] Pakula T, Saijo K, Hashimoto T. Macromolecules 1985;18:2037.
[28] Gorce J, Hellgeth JW, Ward TC. Polym Eng Sci 1993;33:18.